

Brain metabolic correlates of dopaminergic degeneration in de novo idiopathic Parkinson's disease

Valentina Berti · Cristina Polito · Silvia Ramat · Eleonora Vanzi ·
Maria Teresa De Cristofaro · Giannantonio Pellicanò · Francesco Mungai ·
Paolo Marini · Andreas Robert Formiconi · Sandro Sorbi · Alberto Pupi

Received: 22 April 2009 / Accepted: 6 August 2009 / Published online: 2 September 2009
© Springer-Verlag 2009

Abstract

Purpose The aim of the present study was to evaluate the reciprocal relationships between motor impairment, dopaminergic dysfunction, and cerebral metabolism (rCMRglc) in de novo Parkinson's disease (PD) patients.

Methods Twenty-six de novo untreated PD patients were scanned with ^{123}I -FP-CIT SPECT and ^{18}F -FDG PET. The dopaminergic impairment was measured with putaminal ^{123}I -FP-CIT binding potential (BP), estimated with two different techniques: an iterative reconstruction algorithm (BP_{OSEM}) and the least-squares (LS) method (BP_{LS}). Statistical parametric mapping (SPM) multiple regression analyses were performed to determine the specific brain regions in which UPDRS III scores and putaminal BP values correlated with rCMRglc.

Results The SPM results showed a negative correlation between UPDRS III and rCMRglc in premotor cortex, and a positive correlation between BP_{OSEM} and rCMRglc in premotor and dorsolateral prefrontal cortex, not surviving at multiple comparison correction. Instead, there was a positive significant correlation between putaminal BP_{LS} and rCMRglc in premotor, dorsolateral prefrontal, anterior prefrontal, and orbitofrontal cortex ($p < 0.05$, corrected for multiple comparison).

Conclusions Putaminal BP_{LS} is an efficient parameter for exploring the correlations between PD severity and rCMRglc cortical changes. The correlation between dopaminergic degeneration and rCMRglc in several prefrontal regions likely represents the cortical functional correlate of the dysfunction in the motor basal ganglia-cortical circuit in PD. This finding suggests focusing on the metabolic course of these areas to follow PD progression and to analyze treatment effects.

Keywords Parkinson's disease · FP-CIT · FDG · Basal ganglia

Introduction

Parkinson's disease (PD) is a progressive neurodegenerative disorder characterized clinically by bradykinesia, rigidity, resting tremor, and postural instability [1].

The cardinal pathological feature of PD is the degeneration of dopaminergic nigrostriatal neurons in the substantia nigra pars compacta, resulting in a loss of dopaminergic terminals in the striatum [2]. Imaging with single photon emission computed tomography (SPECT) and positron emission tomography (PET) has been widely used to reveal abnormalities in dopaminergic transmission, particularly in the diagnostic phase [3]. Currently, presynaptic SPECT imaging with ^{123}I -FP-CIT (*N*- ω -fluoropropyl-2 β -carbomethoxy-3 β -{4-iodophenyl}-nortropine) is the diagnostic technique most widely used in clinical practice to evaluate dopaminergic system integrity [4, 5] and several studies have shown an inverse correlation between striatal ^{123}I -FP-CIT uptake and motor impairment in PD [6].

Nigrostriatal dopaminergic neuronal loss in PD is, however, the cardinal of several neuro-functional steps in

V. Berti (✉) · C. Polito · E. Vanzi · M. T. De Cristofaro ·
G. Pellicanò · F. Mungai · A. R. Formiconi · A. Pupi
Department of Clinical Pathophysiology, University of Florence,
Viale Morgagni 85,
50134 Florence, Italy
e-mail: valentina.berti@unifi.it

S. Ramat · P. Marini · S. Sorbi
Department of Psychiatric and Neurological Sciences,
University of Florence,
Viale Morgagni 85,
50134 Florence, Italy

the pathologic progression of the disease [7–9]. Previous ^{18}F -FDG PET studies showed a characteristic pattern of regional glucose metabolism (rCMRglc) in patients with PD compared to controls, involving parietal and occipital areas, and dorsolateral prefrontal cortex (DLPFC) [10]. A number of reports also described the expression of an abnormal PD-related metabolic pattern, characterized by increased pallido-thalamic and pontine activity, associated with reductions in lateral frontal, paracentral, inferior parietal, and parieto-occipital regions [11–13]. Several studies also showed the correlation between regional cortical hypometabolism and severity of motor impairment in PD, demonstrating an inverse correlation involving in particular anterior cingulate gyrus, orbitofrontal and occipitotemporal regions [14].

However, to our knowledge, no study has focused specifically on the relation between the severity of dopaminergic degeneration, as assessed with ^{123}I -FP-CIT SPECT, and metabolic dysfunction in PD patients. This approach might reveal in which regions rCMRglc changes are directly related to the dopaminergic neuronal loss.

To this aim, an accurate measurement of dopaminergic degeneration plays a key role. It is known that the quantification of striatal ^{123}I -FP-CIT uptake with the measurement of the binding potential (BP) [15, 16], even if performed with iterative algorithms, is affected by partial volume effects (PVE), which causes an underestimation of BP values [17]; the least squares (LS) method, an algorithm previously developed at our institute, allows one to obtain BP estimates that are less affected by PVE and its reliability has been validated in phantom [17] and clinical studies [18].

Moreover, the enrollment of drug-naïve PD patients is mandatory because in de novo PD patients the pathological processes are not yet affected by pharmacological agents [19], allowing a more accurate insight of PD processes.

Therefore, the present study evaluates in de novo PD patients the relation between the brain metabolic changes, measured with ^{18}F -FDG PET, and the severity of dopaminergic degeneration, assessed with ^{123}I -FP-CIT SPECT. Striatal ^{123}I -FP-CIT uptake was quantified with the BP measurement [15, 16] that was estimated with two different techniques: with an iterative reconstruction algorithm (Ordered Subset Expectation Maximization, OSEM), and with the LS method.

Materials and methods

Patients and clinical scoring

The study included 26 consecutive right-handed de novo PD patients (17 male and nine female, mean age: 65.3 ± 6.4 years) who were examined with magnetic resonance

imaging (MRI) scan, ^{123}I -FP-CIT SPECT and ^{18}F -FDG PET at our university institution. Clinical inclusion criteria were the diagnosis of possible PD according to Gelb criteria [1]. Exclusion criteria were present or past therapy for PD. Nineteen subjects of the present series overlap with those described in a previous ^{123}I -FP-CIT SPECT study [18].

Clinical severity of disease was assessed with Hoehn & Yahr (H&Y) scores [20] and the motor part (part III) of the Unified PD Rating Scale (UPDRS III) [21]. Before the beginning of specific therapy for PD, MRI scan, ^{123}I -FP-CIT, and ^{18}F -FDG were performed. The study was performed under the rules of the Institutional Ethical Committee.

Demographic data, duration of disease, side of motor symptoms onset, UPDRS III scores, and H&Y scores are shown in Table 1.

Imaging procedures

^{123}I -FP-CIT SPECT

All subjects underwent a ^{123}I -FP-CIT SPECT scan. SPECT images were acquired 3 h after intravenous administration of ^{123}I -FP-CIT (185 MBq) with a three-headed camera (IRIX, Philips Medical System, Europe) equipped with UHR collimators. Images were acquired over 360 (120 angles, 40 projection/head, 128×128 matrix, bin size 2.33 mm); scanning time was of 60 s/step and lasted 40 min. Image data were reconstructed using OSEM algorithm (five subsets, eight iterations) [22] into 128 slice (128×128 matrix, 2.33 mm/pixel, 2.33 mm slice thickness). Attenuation correction was performed using Chang algorithm [23] ($\mu = 0.12 \text{ cm}^{-1}$).

MRI

MRI brain scan was performed on Gyroscan NT Intera (Philips Medical System, Europe) with T1-, T2-weighted, and FLAIR sequences (matrix 512×512 , voxel size $0.49 \times 0.49 \times 6.60$ mm). Images were reconstructed into 20 slices

Table 1 Patients' demographic and clinical data

Demographics	Value
Age (years)	65 ± 6 [53–77]
Sex	17 males, 9 females
Side of motor symptoms onset	13 right, 13 left
Symptom at onset	20 tremor, 6 brad/trig
Disease duration (months)	19 ± 9 [3–36]
UPDRS III score	14 ± 5 [7–27]
H&Y score	1.6 ± 0.4 [1–2.5]

Values are mean \pm standard deviation [range]

with 6-mm slice thickness in axial, coronal, and sagittal orientation.

¹²³I-FP-CIT SPECT-MRI Coregistration

Each MRI scan was coregistered with the corresponding SPECT scan reconstructed with the OSEM algorithm by using a 3D method based on rigid transformation with correlation ratio as cost function implemented in Medical Image Processing, Analysis and Visualization (MIPAV version 3.1.3, National Institutes of Health, NIH, Bethesda, MD). An optimization for spatial alignment was performed using anatomic landmarks followed by a least-squares algorithm [24]. Coregistered MRI/SPECT images consisted of 128 axial slices. (128×128 matrix, 2.33 mm/pixel, 2.33 mm slice thickness).

¹⁸F-FDG PET

PD patients were scanned with ¹⁸F-FDG PET. Patients were injected with a dose of 370 MBq ¹⁸F-FDG, in resting state in the eyes-ears open condition, in a dimly lit room with minimal background noise. Thirty minutes after ¹⁸F-FDG administration, a scan lasting 20 min was acquired, using a GE Advance PET scanner (General Electric; Milwaukee, WI), equipped with 18-ring bismuth germanate (BGO) crystals. A polycarbonate head holder was used to reduce head movements during the scan. Emission scans were acquired in two-dimensional mode with an axial FOV of 15 cm and a planar FOV of 55×55 cm. Images were reconstructed by OSEM iterative algorithm (two iterations, 21 subsets). A transmission scan with ⁶⁸Ge-sources was used for photon attenuation correction. Thirty-five PET slices were acquired using a 256×256 matrix with a pixel dimension of 2.15 mm and slice thickness of 4.25 mm.

Image analysis

ROIs on ¹²³I-FP-CIT SPECT

ROIs were manually segmented on the coregistered MRI images on right and left caudate nucleus and right and left putamen, as regions of specific binding, and on cerebellum, as region of non-specific binding. They were rigidly transferred on ¹²³I-FP-CIT SPECT and used for the analyses with both OSEM algorithm and LS method. The skull profile was segmented too and used as the profile of the attenuation map.

LS method

The LS method [25] is an algorithm for measuring ROI activities directly from projections instead of using recon-

structed images. This method has an inherent capability of partial volume effects correction and permits to retrieve unbiased ROI concentration estimates [17]. In this method, each ROI is assumed to have an homogeneous activity concentration and ROIs are treated as the basic image volume elements (also called “natural voxel”) so that the number of unknowns in the tomographic problem is reduced to the number of ROIs (i.e., six, right and left caudate nucleus, right and left putamen, cerebellum and background) instead of the number of all standard voxels (i.e., 128×128×128).

ROIs’ activity concentrations are evaluated with a least-squares procedure where the system matrix is constituted by “ROIs’ sinograms”, which are the sinograms obtained by back-projecting segmented ROIs by taking into account geometrical model of the acquisition system [26] and attenuation effect (Chang model $\mu=0.12\text{ cm}^{-1}$).

¹²³I-FP-CIT SPECT parameter estimate

Striatal BP was estimated on OSEM reconstructed images (BP_{OSEM}) and with LS algorithm (BP_{LS}) as the ratio of a region of specific binding (striatum) to a region of non-specific binding (cerebellum). We estimated BP for right and left caudate nuclei and right and left putamen separately.

Among all striatal regions, putaminal BP was identified as the most accurate measure for determining the severity of dopaminergic degeneration [5, 27] and therefore used to test the correlation with the clinical scales of disease severity and with rCMRglc.

Statistical analysis

All statistical analyses were made using SPSS 15.0 (SPSS Inc., Chicago, IL). Values of $p<0.05$ were considered statistically significant.

PET images were converted from DICOM into Analyze format using the MIPAV software and then processed using SPM5 (Wellcome Department of Cognitive Neurology, Institute of Neurology, London) running on Matlab 7 (Mathworks, Inc., Natick, MA). A 12-parameter linear affine transformation and a non-linear three-dimensional deformation were applied to each subject scan to realign and spatially normalize images to a reference stereotactic template (Montreal Neurological Institute -MNI-, McGill University, Montreal, Quebec). The normalized data were then smoothed using a Gaussian kernel at FWHM 12 mm to account for individual variability in structure-function relation and to enhance the signal-to-noise ratio. Global normalization was performed using the proportional scaling routine in SPM. The gray matter threshold was set to 0.8 of the mean and global calculation was obtained with respect to the mean voxel value.

The multiple regression design was employed to explore regions in which rCMRglc correlates negatively with UPDRS III and positively with putaminal BP_{OSEM} and BP_{LS}. The SPM{t} maps were obtained at a height threshold of $p < 0.005$, cluster extent ≥ 50 voxels. Correction for multiple comparisons was conducted using SPM's small-volume-correction (SVC) facility [28] across the frontal lobe, based on the a priori knowledge of the physiology of fronto-striatal circuits [29, 30] and of the regional pattern of metabolic changes in PD, which involves prefrontal regions [12]. The significance threshold was set to a corrected value of $p < 0.05$ (False Discovery Rate, FDR, corrected).

Coordinates of local maxima were converted from MNI to Talairach space using the "mni2tal" function (<http://www.mrc-cbu.cam.ac.uk/Imaging/Common/mnispace.shtml>) and labeled according to the Talairach and Tournoux space [31] by using the Talairach Daemon Client Version 2.0 (<http://ric.uthscsa.edu/projects/talairachdaemon.html>).

Results

Caudate and putaminal BP_{OSEM} and BP_{LS} values are shown in Table 2.

SPM analysis demonstrated a negative correlation between UPDRS III scores and rCMRglc in bilateral premotor cortex (PMC, Brodmann Area-BA 6) (Table 3). The clusters did not survive after SVC correction for multiple comparisons.

SPM analysis showed a positive correlation between right putaminal BP_{OSEM} and rCMRglc in right DLPFC (BA 9) and right PMC (BA 6); left putaminal BP_{OSEM} positively correlated with rCMRglc in left DLPFC (BA 9) and left PMC (BA 6) (Table 3). The clusters did not survive after SVC correction for multiple comparisons.

Table 2 Striatal BP_{OSEM} and BP_{LS} values

Striatal region	BP _{OSEM}	BP _{LS}	Significance
Right caudate nucleus	3.10±0.77	6.98±1.88	** $p < 0.001$
Left caudate nucleus	3.11±0.75	6.86±1.90	** $p < 0.001$
Right putamen	1.70±0.71	4.59±1.33	** $p < 0.001$
Left putamen	1.79±0.66	4.54±1.33	** $p < 0.001$
Ipsi caudate nucleus	3.28±0.75	7.20±1.82	** $p < 0.001$
Contr caudate nucleus	2.93±0.73	6.64±1.91	** $p < 0.001$
Ipsi putamen	2.03±0.68	5.05±1.36	** $p < 0.001$
Contr putamen	1.47±0.56	4.09±1.36	** $p < 0.001$

Values are mean ± standard deviation

Abbreviations: *Ipsi* Ipsilateral to the most affected body side; *Contr* Contralateral to the most affected body side

Right putaminal BP_{LS} positively correlated with rCMRglc in bilateral DLPFC (BA 9), bilateral PMC (BA 6), and bilateral anterior prefrontal cortex (APFC, BA 10) (Table 3) (Fig. 1). After SVC correction for multiple comparison, right putaminal BP_{LS} positively correlated with rCMRglc in right DLPFC (BA 9), right PMC (BA 6) and right APFC (BA 10).

Left putaminal BP_{LS} positively correlated with rCMRglc in bilateral DLPFC (BA 9), bilateral PMC (BA 6), bilateral APFC (BA 10), and bilateral orbitofrontal cortex (OFC, BA 11) (Table 3) (Fig. 1). After SVC correction for multiple comparison, left putaminal BP_{LS} positively correlated with rCMRglc in left DLPFC (BA 9), left PMC (BA 6), left APFC (BA 10), and left OFC (BA 11).

Discussion

In this study a group of de novo PD patients was examined, by focusing on the reciprocal relationships existing between motor impairment, dopaminergic degeneration severity, and rCMRglc. We studied drug-naive patients in order to capture functional changes uniquely related to the disease process, without any additional confounding effect due to interfering pharmacological action [32].

¹²³I-FP-CIT SPECT striatal BP values were evaluated using both the OSEM algorithm and LS method in order to join LS results with those of a widely employed method in clinical practice, such as OSEM.

Both estimating BP with OSEM reconstructed images and with LS algorithm there were lower BP values in striatal regions contralateral to the first and most affected body side, confirming the asymmetric uptake of ¹²³I-FP-CIT in the PD striatum, previously reported by other studies [5, 33, 34]. Moreover, compared to caudate BP, putaminal BP was significantly more impaired, in accordance with previous SPECT imaging studies [18, 35].

In the SPM multiple regression analysis, the correlation between both clinical measure (UPDRSIII) and rCMRglc, and traditional striatal BP estimate (BP_{OSEM}) and rCMRglc did not survive after correction for multiple comparison, therefore these results will not be further discussed. Instead, the positive correlation between BP_{LS} and rCMRglc survived FDR correction in PMC, DLPFC, APFC, and OFC.

Our results suggest an advantage of BP_{LS} over clinically based assessment, such as UPDRS III, or less sensitive methods, such as BP_{OSEM}, related to the potential for finding a significant correlation even in a relatively small group of patients [36]. Further studies are necessary to evaluate if, with a greater number of subjects, the correlation would be found even with UPDRS III and BP_{OSEM}.

The correlation between disease severity, as measured by BP_{LS}, and functional activity in prefrontal cortical areas

Table 3 List of local maxima of the most significant correlations with rCMRglc

	Cluster extent	Anatomic area	Functional area	Talairach coordinates			t
				x	y	z	
UPDRS III negative							
	94	Left frontal lobe	GFm BA 6	-26	15	62	391
		Left frontal lobe	GFs BA 6	-16	22	60	367
		Left frontal lobe	GFs BA 6	-18	13	64	317
	113	Right frontal lobe	GFs BA 6	22	-6	70	362
		Right frontal lobe	GFs BA 6	16	3	68	351
Right putaminal BP _{OSEM} positive							
	195	Right frontal lobe	GFi BA 9	59	16	22	346
		Right frontal lobe	GFm BA 9	55	21	31	337
		Right frontal lobe	GPrC BA 6	56	1	28	314
Left putaminal BP _{OSEM} positive							
	213	Left frontal lobe	GFm BA 9	-22	32	28	475
	76	Left frontal lobe	GPrC BA 6	-44	2	37	336
Right putaminal BP _{LS} positive							
	2552	Right frontal lobe	GFs BA 9	16	48	25	4.93*
		Right frontal lobe	GFd BA 10	2	51	9	4.47*
		Right frontal lobe	GFs BA 10	12	66	2	4.30*
	2035	Right frontal lobe	GFi BA 6	55	0	24	4.77*
		Right frontal lobe	GFm BA 9	50	25	32	4.72*
	1251	Left frontal lobe	GPrC BA 9	-44	21	36	463
		Left frontal lobe	GPrC BA 6	-53	0	35	443
	178	Left frontal lobe	GFm BA 10	-38	53	10	415
Left putaminal BP _{LS} positive							
	1332	Left frontal lobe	GPrC BA 9	-46	21	36	5.62*
		Left frontal lobe	GFm BA 9	-24	32	26	4.69*
		Left frontal lobe	GPrC BA 6	-48	0	33	4.62*
	454	Right frontal lobe	GFs BA 11	8	59	-21	498
		Left frontal lobe	GFs BA 11	-2	57	-21	3.77*
		Left frontal lobe	GFs BA 11	-12	66	-10	363
	125	Left frontal lobe	GFm BA 10	-38	51	9	3.77*
	362	Right frontal lobe	GPrC BA 6	55	2	31	375
	175	Left frontal lobe	GFs BA 9	-18	58	27	365
		Left frontal lobe	GFs BA 10	-12	61	23	342
	675	Right frontal lobe	GFd BA 10	4	51	5	347
		Right frontal lobe	GFd BA 9	20	42	22	343
	101	Right frontal lobe	GR BA 11	4	32	-20	331

*Survived at SVC correction for multiple comparisons ($p < 0.05$)

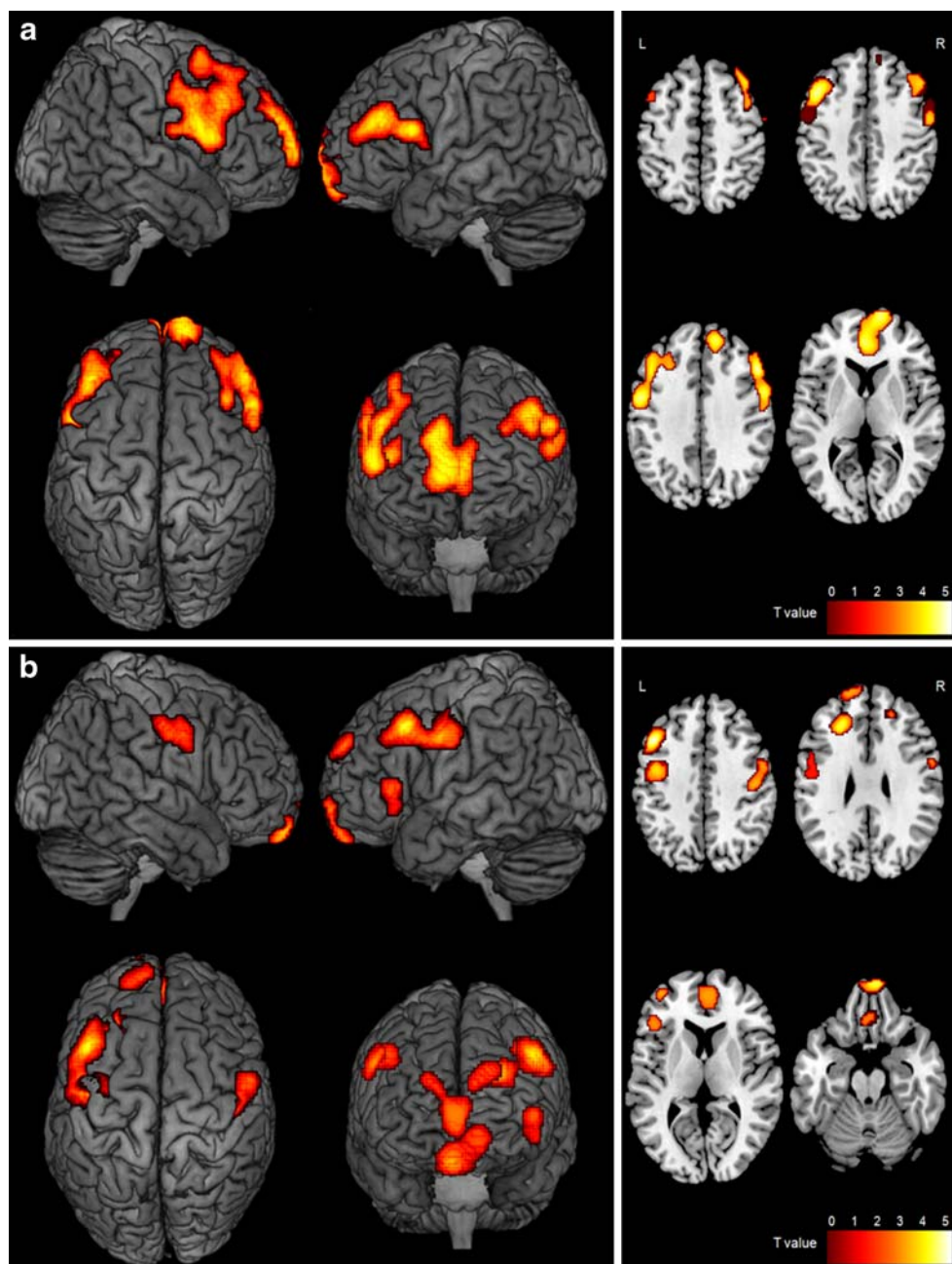
Abbreviations: *GFm* Middle frontal gyrus; *GFs* Superior frontal gyrus; *GFi* Inferior frontal gyrus; *GPrC* Precentral gyrus; *GFd* Medial frontal gyrus; *GR* Rectal gyrus

confirms the classical model of the basal ganglia circuit organization, derived from anatomical and electrophysiological studies in non-human primates [37, 38]. Indeed, the organization of the corticostriatal circuits [29, 30] involves the processing of descending cortical information that is relayed back to frontal motor areas through motor nuclei of the basal ganglia via the thalamus. This anatomical

segregation was also observed in humans with MRI tractography studies that revealed motor projections from putamen to the primary motor area, primary somatosensory area, and PMC [39].

The essential pathophysiological characteristic of the PD state is increased neuronal firing activity in the output nuclei of the basal ganglia leading to excessive inhibition of

Fig. 1 Regions with significantly positive correlation with right (**a**) and left (**b**) BP_{LS} in the ^{18}F -FDG study



thalamocortical motor system [40]. Our results therefore confirm pathophysiological changes occurring in the functional organization of the basal ganglia in PD, since the excessive inhibition of thalamocortical projections may be at the basis of reduced prefrontal rCMRglc correlating with reduced BP.

In this study we found a positive correlation between putaminal BP_{LS} and rCMRglc not only in frontal regions belonging to the motor loop, but also in dorsolateral, anterior prefrontal, and orbitofrontal regions, which are part of the associative and limbic loop [29]. Indeed, the loss of dopaminergic projections in PD is not confined

to the putamen but at the same time also occurs in the caudate nucleus and in ventral striatum, which are the striatal relays of associative and limbic frontostriatal loops, therefore connected with DLPFC, APFC, and OFC. Even if our patients are in the early stages of PD, the caudate nucleus has already been involved in the disease process, as demonstrated by the correlation between putaminal and caudate BP, with both the reconstruction algorithms used.

To our knowledge, few studies focused on the correlation between disease severity and rCMRglc using voxel-based SPM multiple regression analyses [14, 41], showing

an inverse correlation between UPDRS III and rCMRglc not only in the OFC and APFC but also in the primary and associative visual cortex [14]. The correlation of these additional areas may be the effect of a more extended striatal dopaminergic deficit, due to a PD sample less homogeneous and with a wider range of disease severity in those studies than that of the preset study, which includes only de novo PD patients.

Spatial covariance methods, based on principal component analysis (PCA), were instead used in several previous ^{18}F -FDG PET studies [41, 42], which identified a PD-related pattern characterized by increased pallidothalamic and pontine metabolic activity associated with relative metabolic reductions in the PMC, supplementary motor areas and parieto-occipital association regions; the expression of this pattern has been found to correlate with standardized motor ratings [11, 42–44]. The network PCA analysis has been also used to assess the correlation between ^{18}F -DOPA and ^{18}F -FDG by Kaasinen and Coll. [34], showing that the dopaminergic impairment was associated with decreased FDG uptake in cerebellum and thalamus, and increased FDG uptake in motor cortex; in the same study the univariate analysis of correlation (SPM) between the two tracers did not produce any significant relationship.

Our findings are only partially in accordance with these results, since we found a metabolic impairment associated with dopaminergic degeneration in prefrontal areas, as in the PD-related pattern [42–44]. However, we found neither increased FDG uptake in motor cortex [34] nor metabolic variations in subcortical regions [34, 42–44].

These differences may be due to the different statistical approach employed [45] but also to the inclusion in the PD series of these studies of patients at different disease stages some of which already under medication. Besides, the presence of hypermetabolism in subcortical regions and motor cortex is still under debate, since several autoradiographic studies with 2-deoxyglucose in PD animal models did not confirm increased glucose consumption in cortical or subcortical regions [46, 47].

To our knowledge, this is the first study that reports the correlation between ^{123}I -FP-CIT and rCMRglc, demonstrating a direct association between a biomarker of dopaminergic degeneration severity and cortical metabolic reduction in several frontal and prefrontal areas, such as PMC, DLPFC, APFC, and OFC, which are involved in different aspects of motor, cognitive, and behavioral control [48]. Besides, this approach demonstrates the involvement of dorsolateral prefrontal and orbitofrontal areas not directly belonging to the frontostriatal motor loop but to the associative and the limbic loop, suggesting that even in early PD stages, non-motor circuits begin to be affected by the disease. This finding is in the line of recent views

connecting degenerative diseases [49] and it will be object of our future investigation.

Finally, given the recent great interest for imaging biomarkers, in particular for neurodegenerative diseases, our findings turn attention to ^{18}F -FDG uptake in prefrontal regions as a potential biomarker in PD. A biomarker is a characteristic that is objectively measured and evaluated as an indicator of normal or pathogenic biological processes [50]. According with this, prefrontal ^{18}F -FDG uptake might fulfill the basic requirements for a biomarker, since it can be objectively measured and it is associated with the PD pathogenic process, i.e., the dopaminergic degeneration as demonstrated in this study. Additional studies are necessary to complete the evaluation of the possible use of ^{18}F -FDG PET as an imaging biomarker in PD.

In conclusion, our results in de novo PD patients demonstrated that putaminal BP values, measured with the LS method, could be a sensitive parameter to explore correlations with rCMRglc. The finding that several prefrontal areas are the cortical regions most directly affected by dopaminergic degeneration suggests focusing attention on the metabolic course of these areas, not only to follow the progression of PD functional changes but also to analyze treatment effects. Further studies are necessary to confirm our results in a larger series of de novo PD patients and to evaluate future applications.

References

1. Hughes A, Daniel SE, Kilford L, Lees AJ. Accuracy of clinical diagnosis of idiopathic Parkinson's disease: a clinico-pathological study of 100 cases. *J Neurol Neurosurg Psychiatry*. 1992;55:181–4.
2. Fearnley JM, Lees AJ. Ageing and Parkinson's disease: substantia nigra regional selectivity. *Brain*. 1991;114:2283–301.
3. Seibyl JP. Imaging studies in movement disorders. *Semin Nucl Med*. 2003;33:105–13.
4. Booij J, Speelman JD, Horstink MWIM, Wolters EC. The clinical benefit of imaging striatal dopamine transporters with [^{123}I]FP-CIT SPET in differentiating patients with presynaptic parkinsonism from those with other forms of parkinsonism. *Eur J Nucl Med*. 2001;28:266–72.
5. Spiegel J, Hellwig G, Samnick S, Jost W, Mollers MO, Fassbender K, et al. Striatal FP-CIT uptake differs in subtypes of early Parkinson's disease. *J Neural Transm*. 2007;114:331–5.
6. Marshall V, Grosset D. Role of dopamine transporter imaging in routine clinical practice. *Mov Disord*. 2003;18:1415–23.
7. Bezdard E, Gross CE, Brotchie JM. Presymptomatic compensation in Parkinson's disease is not dopamine-mediated. *Trends Neurosci*. 2003;26:215–21.
8. Braak H, Del Tredici K, Bratzke H, Hamm-Clement J, Sandmann-Keil D, Rüb U. Staging of the intracerebral inclusion body pathology associated with idiopathic Parkinson's disease (preclinical and clinical stages). *J Neurol*. 2002;249(Suppl 3):III/1–5.
9. Obeso JA, Rodriguez-Oroz MC, Lanciego JL, Rodriguez Diaz M. How does Parkinson's disease begin? The role of compensatory mechanisms. *Trends Neurosci*. 2004;27:125–7.

10. Eckert T, Barnes A, Dhawan V, Frucht S, Gordon MF, Feigin AS, et al. FDG PET in the differential diagnosis of parkinsonian disorders. *NeuroImage*. 2005;26:912–21.
11. Eidelberg D, Moeller JR, Dhawan V, Spetsieris P, Takikawa S, Ishikawa T, et al. The metabolic topography of parkinsonism. *J Cereb Blood Flow Metab*. 1994;14:783–801.
12. Fukuda M, Edwards C, Eidelberg D. Functional brain networks in Parkinson's disease. *Parkinsonism and Related Disorders*. 2001;8:91–4.
13. Huang C, Tang C, Feigin A, Lesser M, Ma Y, Pourfar M, et al. Changes in network activity with the progression of Parkinson's disease. *Brain*. 2007;130:1834–46.
14. Nagano-Saito A, Kato T, Arahata Y, Washimi Y, Nakamura A, Abe Y, et al. Cognitive- and motor-related regions in Parkinson's disease: FDOPA and FDG PET studies. *NeuroImage*. 2004;22:553–61.
15. Tissingh G, Booij J, Bergmans P, Winogrodzka A, Janssen A, Van Royen E, et al. Iodine-123-N-fluoropropyl-2-β-carbomethoxy-3β-(4-iodophenyl)tropane SPECT in healthy controls and early stage, drug-naïve Parkinson's disease. *J Nucl Med*. 1998;39:1143–8.
16. Innis RB, Cunningham VJ, Delforge J, Fujita M, Gjedde A, Gunn RN, et al. Consensus nomenclature for in vivo imaging of reversibly binding radioligands. *J Cereb Blood Flow Metab*. 2007;27:1533–9.
17. Vanzi E, De Cristofaro MT, Ramat S, Sotgia B, Mascalchi M, Formiconi AR. A direct ROI quantification method for inherent PVE correction: accuracy assessment in striatal SPECT measurements. *Eur J Nucl Med Mol Imaging*. 2007;34:1480–9.
18. Berti V, Pupi A, Ramat S, Vanzi E, De Cristofaro MT, Pellicano G, et al. Clinical correlation of the binding potential with ¹²³I-FP-CIT in de novo idiopathic Parkinson's disease patients. *Eur J Nucl Med Mol Imaging*. 2008;35:2220–6.
19. Fahn S, Oakes D, Shoulson I, Kieburtz K, Rudolph A, Lang A, et al. Levodopa and the progression of Parkinson's disease. *N Engl J Med*. 2004;351:2498–508.
20. Hoehn MM, Yahr MD. Parkinsonism: onset, progression and mortality. *Neurology*. 1967;17:427–42.
21. Fahn S, Elton RL. and members of the UPDRS Development Committee. Unified Parkinson's disease rating scale. In: Fahn S, Marsden CD, Calne DB, Goldstein M, editors. Recent development in Parkinson's disease. Florham Park: Macmillan Healthcare information; 1987. pp. 153–64.
22. Hudson HM, Larkin RS. Accelerated image reconstruction using ordered subsets of projection data. *IEEE Trans Med Imaging*. 1994;13:601–9.
23. Chang L. A method for attenuation correction in computed tomography. *IEEE Trans Nucl Sci*. 1987;25:638–64.
24. Arun KS, Huang TS, Blostein S. Least-squares of two 3d point sets. *IEEE Trans Pattern Anal Mach Intell*. 1987;9:698–700.
25. Formiconi AR. Least squares algorithm for region of interest evaluation in emission tomography. *IEEE Trans Med Imag*. 1993;12:90–100.
26. Formiconi AR, Passeri A, Calvini P. Theoretical determination of the collimator geometrical transfer function for the reconstruction of SPECT data. *IEEE Trans Nucl Sci*. 1999;46:1075–80.
27. Isaias IU, Benti R, Cilia R, Canesi M, Marotta G, Gerundini P, et al. [¹²³I]FP-CIT striatal binding in early Parkinson's disease patients with tremor vs. akinetic-rigid onset. *NeuroReport*. 2007;18:1499–502.
28. Worsley K, Marrett S, Neelin P, Vanda A, Friston K, Evans A. A unified statistical approach for determining significant signals in images of cerebral activation. *Human Brain Mapping*. 1996;4:58–73.
29. Alexander GE, DeLong MR, Strick PL. Parallel organization of functionally segregated circuits linking basal ganglia and cortex. *Ann Rev Neurosci*. 1986;9:357–81.
30. Alexander GE, Crutcher MD. Functional architecture of basal ganglia circuits: neural substrates of parallel processing. *Trends Neurosci*. 1990;13:266–71.
31. Talairach J, Tournoux P. Co-planar stereotaxic atlas of the human brain. New York: Thieme; 1988.
32. Hirano S, Asanuma K, Ma Y, Tang C, Feigin A, Dhawan V, et al. Dissociation of metabolic and neurovascular responses to levodopa in the treatment of Parkinson's disease. *J Neurosci*. 2008;28:4201–9.
33. Eshuis SA, Maguire RP, Leenders KL, Jonkman S, Jager PL. Comparison of FP-CIT SPECT with F-DOPA PET in patients with de novo and advanced Parkinson's disease. *Eur J Nucl Med Mol Imaging*. 2006;33:200–9.
34. Kaasinen V, Maguire RP, Hundemer HP, Leenders KL. Corticostriatal covariance patterns of 6-[¹⁸F]fluoro-L-dopa and [¹⁸F]fluorodeoxyglucose PET in Parkinson's disease. *J Neurol*. 2006;253:340–8.
35. Benamer HTS, Patterson J, Wyper DJ, Hadley DM, Macphee GJ, Grosset DG. Correlation of Parkinson's disease severity and duration with ¹²³I-FP-CIT SPECT striatal uptake. *Mov Disord*. 2000;15:692–8.
36. Alexander GE, Chen K, Pietrini P, Rapoport SI, Reiman EM. Longitudinal PET evaluation of cerebral metabolic decline in dementia: a potential outcome measure in Alzheimer's disease treatment studies. *Am J Psychiatry*. 2002;159:738–45.
37. Albin R, Young AB, Penny JB. The functional anatomy of basal ganglia disorders. *Trends Neurosci*. 1989;12:366–75.
38. Obeso JA, Rodriguez-Oroz MC, Rodriguez M, Lanciego JL, Artieda J, Gonzalo N, et al. Pathophysiology of the basal ganglia in Parkinson's disease. *Trends Neurosci*. 2000;23:18–19.
39. Leh SE, Pfitto A, Chakravarty MM, Strafella AP. Fronto-striatal connections in the human brain: a probabilistic diffusion tractography study. *Neurosci Lett*. 2007;419:113–8.
40. Obeso JA, Marin C, Rodriguez-Oroz C, Blesa J, Benitez-Temino B, Mena-Segovia J, et al. The basal ganglia in Parkinson's disease: current concepts and unexplained observations. *Ann Neurol*. 2008;64:S30–46.
41. Lozza C, Marié RM, Baron JC. The metabolic substrates of bradykinesia and tremor in uncomplicated Parkinson's disease. *Neuroimage*. 2002;17:688–99.
42. Eckert T, Tang C, Eidelberg D. Assessment of the progression of Parkinson's disease: a metabolic network approach. *Lancet Neurol*. 2007;6:926–32.
43. Carbon M, Eidelberg D. Modulation of regional brain function by deep brain stimulation: studies with positron emission tomography. *Curr Opin Neurol*. 2002;15:451–5.
44. Lozza C, Baron JC, Eidelberg D, Mentis MJ, Carbon M, Marié RM. Executive processes in Parkinson's disease: FDG-PET and network analysis. *Hum Brain Mapp*. 2004;22:236–45.
45. Moeller JR, Habeck CG. Reciprocal benefits of mass-univariate and multivariate modeling in brain mapping: applications to event-related functional MRI, H₂¹⁵O-, and FDG-PET. *Int J Biomed Imag* 2006;1–13.
46. Brownell AL, Canales K, Chen YI, Jenkins BG, Owen C, Livni E, et al. Mapping of brain function after MPTP-induced neurotoxicity in a primate Parkinson's disease model. *Neuroimage*. 2003;20(2):1064–75.
47. Meissner W, Guigoni C, Cirilli L, Garret M, Bioulac BH, Gross CE, et al. Impact of chronic subthalamic high-frequency stimulation on metabolic basal ganglia activity: a 2-deoxyglucose uptake and cytochrome oxidase mRNA study in a macaque model of Parkinson's disease. *Eur J Neurosci*. 2007;25(5):1492–500.
48. Utter AA, Basso MA. The basal ganglia: an overview of circuits and function. *Neurosci Biobehav Rev*. 2008;32(3):333–42.
49. Braak H, Rub U, Schultz C, Del Tredici K. Vulnerability of cortical neurons to Alzheimer's and Parkinson's disease. *J Alzheimers Dis*. 2006;9:35–44.
50. Biomarkers Definition Working Group. Biomarkers and surrogate endpoints: preferred definitions and conceptual framework. *Clin Pharmacol Ther*. 2001;69:89–95.